

5-2024

## Dimensionlessly Comparing Hydrogen and Helium Plasmas at LAPD

Lela Creamer  
*William & Mary*

Follow this and additional works at: <https://scholarworks.wm.edu/honorsthesis>



Part of the [Plasma and Beam Physics Commons](#)

---

### Recommended Citation

Creamer, Lela, "Dimensionlessly Comparing Hydrogen and Helium Plasmas at LAPD" (2024).  
*Undergraduate Honors Theses*. William & Mary. Paper 2228.  
<https://scholarworks.wm.edu/honorsthesis/2228>

This Honors Thesis -- Open Access is brought to you for free and open access by the Theses, Dissertations, & Master Projects at W&M ScholarWorks. It has been accepted for inclusion in Undergraduate Honors Theses by an authorized administrator of W&M ScholarWorks. For more information, please contact [scholarworks@wm.edu](mailto:scholarworks@wm.edu).

# Dimensionlessly Comparing Hydrogen and Helium Plasmas at LAPD

A thesis submitted in partial fulfillment of the requirement  
for the degree of Bachelor of Science with Honors in  
Physics from the College of William and Mary in Virginia,

by

Lela B. Creamer

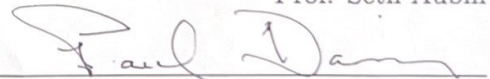
Accepted for Honors  
(Honors or no-Honors)



Advisor: Prof. Saskia Mordijck



Prof. Seth Aubin



Prof. Paul Davies

Williamsburg, Virginia  
May 6, 2024



# Contents

Acknowledgments	iii
List of Figures	iv
List of Tables	v
Abstract	v
<b>1 Introduction</b>	<b>1</b>
1.1 Motivation . . . . .	1
1.2 Characteristics of Plasmas . . . . .	3
1.3 Thesis Goals . . . . .	4
<b>2 Using Dimensionless Numbers to Compare Turbulences</b>	<b>6</b>
2.1 Drift Waves . . . . .	6
2.2 Dimensionless Numbers . . . . .	8
<b>3 Dimensionlessly Matching Plasmas at LAPD</b>	<b>12</b>
3.1 Experimental Setup . . . . .	12
3.2 Langmuir Probes . . . . .	15
3.3 Obtaining Electron Temperature and Density from Langmuir Probes	18
<b>4 Comparing Hydrogen and Helium Plasmas</b>	<b>22</b>

4.1	Dimensionless Matches . . . . .	22
4.2	Partial Dimensionless Matches . . . . .	27
4.3	Calculating the Turbulence Growth Rate . . . . .	27
4.4	Impact of the Magnetic Field on Collisionality . . . . .	31
4.5	Comparing the Density Gradients of Dimensionlessly Matched Plasmas	33
<b>5</b>	<b>Discussion</b>	<b>36</b>
<b>A</b>	<b>File Names and Times of Dimensionless Matches</b>	<b>39</b>

# Acknowledgments

First and foremost, I would like to thank my advisor, Saskia Mordijck, for being a wonderful, patient, and honest mentor throughout my time in her research group. I am also deeply grateful to Leo Murphy for his invaluable help getting me started on this research project, giving me a strong foundation to build on, and answering my many questions along the way. I would also like to thank the many wonderful teachers in William & Mary's Physics department for all the ways they supported me and challenged me to think in ways I didn't know were possible. I am also incredibly grateful for my fellow physics students, who helped me realize that no matter how hard the problem was, I'd be okay if I was surrounded by good people. Beyond the realm of physics, I am eternally grateful to my family for their unending encouragement, kindness, honesty, and support. Listening to me ramble about my research means more to me than you will ever know. And finally, I'm grateful for my friends, who are endlessly inspiring and make me ridiculously happy no matter how stressed I am. Thank you all so, so much.

# List of Figures

1.1	Nonlinear confinement . . . . .	3
3.1	LAPD diagram . . . . .	13
3.2	Density as a function of radial position and time . . . . .	14
3.3	LAPD radial view (with probes) . . . . .	15
3.4	IV sweep . . . . .	16
3.5	Current vs. time . . . . .	17
3.6	Smoothing comparisons . . . . .	20
4.1	Temperature and density profiles of the relative gyroradius and collisionality dimensionless matches . . . . .	24
4.2	Unreliable edge temperatures . . . . .	25
4.3	Radial profiles of the relative gyroradius and collisionality dimensionless matches . . . . .	26
4.4	Temperature and density profiles for the relative gyroradius-only and collisionality-only matches . . . . .	28
4.5	$\rho^*$ and collisionality profiles for the relative gyroradius-only and collisionality-only matches . . . . .	29
4.6	He Collisionality Comparisons . . . . .	31
4.7	He Collisionality Comparisons . . . . .	32
4.8	Density gradient . . . . .	33

# List of Tables

4.1	H/He ratios for average temperature, density, $\rho^*$ , $\nu_{eff}$ , and turbulence growth rate values for partial and total dimensionless matches . . . .	30
4.2	Normalized density gradients . . . . .	34



## **Abstract**

This project compares the hydrogen and helium gas puff plasmas created at the Large Plasma Device (LAPD) using dimensionless numbers to determine the extent to which the turbulence pattern can be explained by plasma physics. Since turbulence tends to dissipate energy and particles in a plasma, it can cause problems for fusion reactors by reducing their efficiency. With a better understanding of turbulence's causes and behavior, some of this energy loss could potentially be avoided. In recent experiments at LAPD, an unexpectedly high amount of turbulence was detected when helium was used to create the plasma, which sparked interest in further research. LAPD is a linear plasma device that creates short bursts of plasma using pulsed discharges and uses probes such as Langmuir probes and Mach probes to measure the properties of the plasma. The hydrogen and helium plasmas were dimensionlessly matched using data from these probes and modified versions of Kadomtsev's dimensionless plasma parameters. At least one solid dimensionless match was found between the hydrogen and helium plasmas, and the two plasmas displayed the expected relationships between density and temperature.

# Chapter 1

## Introduction

### 1.1 Motivation

Physics uses math to describe and predict the world and various systems within it. However, trying to describe the mechanics of the world with absolute precision using math can be ineffective or even impossible. In order to work around this limitation, physicists use assumptions that allow them to simplify the mathematics they use while still describing and predicting key characteristics of that system. For example, a physicist would generally neglect air resistance when trying to calculate how long it would take for a ball to impact the ground when dropped from a height of two meters. However, if the ball were to fall from a much greater height, it would reach terminal velocity, where the forces of gravitational acceleration and air resistance balance out and cause the ball to fall at a constant rate. In the latter case, attempting to calculate the time the ball would hit the ground without taking air resistance into account would lead to an incorrect conclusion even if all other parts of the calculation were correct. This demonstrates that while assumptions can be useful—and even necessary—in physics, they are not universal.

In 2020, King et al. published a scientific paper discussing magnetic confinement in tokamaks which indicated that physicists studying plasmas in space may be making

an incorrect assumption. Many astrophysical plasmas consist primarily of hydrogen but contain a small amount of helium. One example of this is the solar wind, which has a ratio of around 4-5% of helium to hydrogen [1]. These plasmas are frequently modeled as consisting entirely of hydrogen since the effects of helium are thought to be negligible. However, King's paper showed that introducing an additional element (also referred to as an ion species) into the plasma—even in small amounts comparable to the percentage of helium in the solar wind—has notable effects on the behavior of the plasma as a whole [2].

King specifically noted that adding an additional ion species had an impact on the confinement of the plasma. In order to avoid losing energy or damaging equipment, plasmas are often confined using magnetic fields when they are created on Earth. King observed that adding an additional ion species had an impact on the efficiency of this confinement. Furthermore, as shown in Fig. 1.1, the changes in the confinement were not linear, which means that there is an unknown mechanism that causes the confinement to change abruptly at certain thresholds [2]. This indicates that there is a gap in our understanding of fundamental plasma physics.

The purpose of this project is to fill in parts of this gap, by experimentally observing the effect of ion species on turbulence in dimensionlessly matched hydrogen and helium plasmas. Turbulence is a phenomenon that reduces the effectiveness of magnetic confinement in plasmas, which means that the previously observed results of mixed ion species affecting confinement could be linked to or caused by effects on turbulence in the plasma [3]. The method chosen to compare the two plasmas will also reveal the extent to which some other area of physics, such as atomic physics, plays a role in this kind of turbulence.

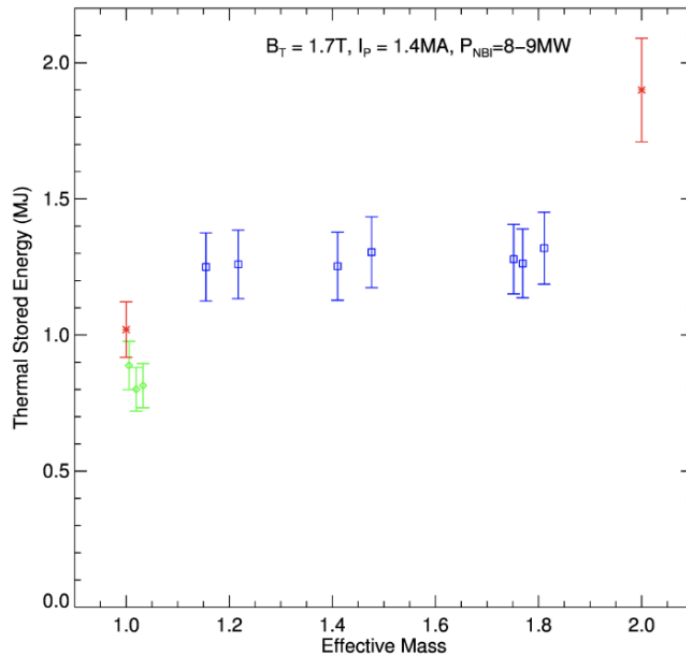


Figure 1.1: Graph comparing the amount of stored thermal energy in a tokamak to the effective mass of mixed hydrogen and deuterium, which varies as the two ion species are mixed. The red markers indicate pure isotope plasmas, the green markers indicate plasmas with very low deuterium content, and the blue markers indicate mixed isotope plasmas [2]. Note how it abruptly rises around the 10-15% mixture range, which is around the amount of helium mixed in to the primarily hydrogen solar wind.

## 1.2 Characteristics of Plasmas

Plasma is an ionized gas in which one or more electrons are stripped away from an atom, usually through heating. This leads to a new state of matter where small, negatively charged electrons and heavier, positively charged ions interact with one another through electric and magnetic fields as well as through collisions. Since many gases contain at least a small fraction of ionized particles, plasmas are further distinguished from gases in that they must exhibit collective behavior [4].

Because plasmas consist of charged particles and are generally produced at high

temperatures, plasmas are often confined using magnetic fields rather than solid surfaces to avoid unnecessary energy loss or equipment damage. Since the plasma is concentrated in a specific location due to this magnetic confinement, density gradients form at the edges of the plasma. These density gradients lead to turbulence [5].

Turbulence is a form of chaotic fluid flow that is characterized by eddies and swirls. These eddies and swirls can vary greatly in size, from Jupiter's red spot to a microscopic scale. Turbulence frequently forms to dissipate gradients such as those caused by magnetic confinement, and it is a major obstacle standing in the way of reliable fusion power due to its ability to dissipate energy and particles into its surroundings substantially faster than what would be possible if the dissipation was caused simply by particle collisions [3]. Its chaotic nature also means that small changes in the initial conditions of a system can cause the end results to vary dramatically, which also makes it more difficult to describe using mathematics.

Drift wave turbulence is a specific form of turbulence that arises from drift waves, which occur in all plasmas with a magnetically produced density gradient. Drift waves are driven by a pressure gradient and move perpendicularly to the magnetic field. When drift waves grow, they become turbulent, and are able to transport particles, energy, and momentum across magnetic field lines [6]. Plasma parameters linked to this kind of turbulence can be scaled up or down without changing the overall behavior of the turbulence through the use of dimensionless numbers.

### **1.3 Thesis Goals**

The end objective of this project is to compare the turbulence in fully hydrogen and fully helium plasmas so that future work can use it as a baseline to examine how mixing ion species affects drift wave turbulence. This project aims to accomplish this goal by dimensionlessly comparing hydrogen and helium plasmas created using a gas

puff at the Large Plasma Device (LAPD) at UCLA. LAPD is a cylindrical plasma device that excels at creating highly repeatable linear plasmas. It offers a high degree of control over many important plasma parameters such as the strength and uniformity of the magnetic field, the amount of current used to produce the plasma, and the presence of neutrals in the plasma. This makes it ideal for studying electrostatic drift waves, since it can produce a constant, axial magnetic field that allows drift waves to occur in their simplest form. It is also a useful experimental device because it offers the use of many diagnostics such as Langmuir probes, Mach probes, and an interferometer. It also has a high-speed camera pointing towards the cathode that can be used to obtain qualitative and quantitative information about how the plasma behaves over time. The plasmas at LAPD were dimensionally matched through one parameter experimentally by doubling the strength of the magnetic field for helium plasmas, and the plasma densities and temperatures were varied for hydrogen and helium plasmas to increase the likelihood of a dimensionless match for the other relevant dimensionless parameter.

Chapter 2 of this thesis will outline the importance and mechanics of drift waves and dimensionless numbers, as well as how they relate to this project. Chapter 3 will explain the experimental setup at LAPD, how experimental data was collected, and how that data was analyzed to gain information about electron density and temperature. Chapter 4 will show dimensionless matches of the hydrogen and helium plasmas. Chapter 5 of this thesis will explain the physical significance of the results and evaluate the extent to which they match theoretical predictions.

# Chapter 2

## Using Dimensionless Numbers to Compare Turbulences

This chapter will explain how dimensionless numbers can be used to compare the drift wave turbulence of hydrogen and helium plasmas at LAPD. First, it will explain drift waves and provide the imaginary component of the dispersion relation for an electrostatic drift wave, which is linked to turbulence. It will then define dimensionless numbers and the dimensionless parameters that are relevant to this system: relative gyroradius and  $\nu_{eff}$ , the relative gyroradius and effective collisionality respectively.

### 2.1 Drift Waves

Drift waves are a form of turbulence that occur in all magnetized plasmas with a pressure gradient, which means that they exist in all magnetically confined plasmas. Drift waves are inherently unstable due to the fact that their density distribution changes more rapidly than the electric potential distribution, which causes the oscillations to grow and become unstable. This leads to drift wave turbulence. Drift wave turbulence is problematic for all plasmas that rely on magnetic confinement, such as tokamaks and stellarators, due to its ability to transport energy and particles perpendicularly to magnetic field lines.

Plasmas are a dispersive medium, which means that different wave frequencies propagate at varying rates throughout the plasma. This can be described using a dispersion relation, which relates the frequency to its wavelength or wave number. The frequencies in dispersion relations also have an imaginary component. This imaginary component describes the rate at which the plasma wave grows or dampens. When waves grow uncontrollably, they become unstable and can lead to turbulence. This unstable growth means that the imaginary component of a dispersion relation can be used as an indicator of turbulence in a plasma. Since plasma waves can propagate through plasma in a variety of ways, not all dispersion relations are the same. This project focuses on the imaginary component of the dispersion relation for an electrostatic drift wave, which can be written as follows:

$$\gamma = \frac{\eta k_{\perp}^2 k_y^2 \nu_{de}^2}{\mu_0 k_z^2 \nu_A^2} \sim \frac{\nu_{ei} k_{\perp}^2 r_{LS}^2 k_y^2 \nu_{de}^2}{k_z^2 \nu_{t,e}^2} \quad (2.1)$$

where  $\gamma$  is the turbulence growth rate,  $\eta$  is the resistivity of the plasma,  $k_{\perp}$  is the perpendicular component of the wave number with respect to the magnetic field (which is taken to be in the  $z$  direction),  $k_y \nu_{de}$  is the approximate frequency for an electron drift wave (composed of the  $y$ -component of the wave number  $\vec{k}$  and the velocity of the electron drift wave respectively),  $\mu_0$  is the vacuum permeability,  $k_z \nu_A$  is the shear Alfvén frequency, composed of the  $z$ -component of the wave number  $\vec{k}$  and the Alfvén velocity,  $\nu_{ei}$  is the electron-ion collision frequency,  $r_{LS}$  is the Larmor radius, and  $\nu_{t,e}$  is the electron thermal velocity. While Eq. 2.1 describes drift waves in a slab geometry, this does not pose a problem when it comes to applying this equation to the cylindrical geometry of LAPD. Both the  $y$  direction and  $\nu_{de}$  correspond to the azimuthal direction of LAPD, and the geometric factors remained constant through all the experiments run in this project.



This equation is valid when  $k_y v_{de} \gg k_z C_s$ , where  $C_s$  is the plasma sound speed. While  $v_{de}$  is not identical to the electron diamagnetic drift velocity when there is a temperature gradient across the magnetic field, they are similar in direction and magnitude. It is important to note that when drift waves are referred to as “electrostatic,” this actually refers to the fact that magnetic perturbations play a negligible role in the behavior of the drift wave [6]. One can observe from looking at this equation that the growth rate increases as the wavelength parallel to the magnetic field increases, which means that drift waves are particularly apparent in long, cylindrical, magnetically confined plasmas such as those created at LAPD.

It is important to note that Eq. 2.1 depends on collisionality, which is dimensionless, and the Larmor radius, which is linked to the dimensionless parameter  $\rho^*$ . If all other parameters in Eq. 2.1 remain constant and the Larmor radius and collisionality of hydrogen and helium plasmas are matched, then the imaginary component of the dispersion relation should remain the same. This matching would lead to similar levels of turbulence.

## 2.2 Dimensionless Numbers

Dimensionless numbers are numbers that describe a property of a physical system without units. They isolate physically significant combinations of parameters and can be used to determine how a given system will respond when these parameters are changed. For instance, dimensionless numbers are used in wind tunnels when scale models of aircraft are tested in lieu of their larger counterparts [9]. Though the sizes of the aircraft are not the same, dimensionlessly matching the two systems means that the larger aircraft should behave the same way as the smaller one.

This is the motivation for using dimensionless numbers in this experiment. While hydrogen and helium plasmas behave differently when they are at similar tempera-

tures, densities, and magnetic fields, they should behave the same way when dimensionlessly matched using equations from plasma physics.

The dimensionless numbers used in this project were derived using the Buckingham Pi theorem. Buckingham Pi theorem is a key theorem in the derivation and use of dimensionless numbers. It states that any physically meaningful system with  $n$  variables and  $k$  dimensions can be described by  $(n-k)$  dimensionless numbers [7]. While the Buckingham Pi theorem can be used to find dimensionless parameters (frequently referred to as Buckingham Pi products), they are not the only possible combinations of plasma parameters that lead to a dimensionless set—and not all dimensionless parameters have equal physical significance. Since the aim of this project is to compare turbulence in hydrogen and helium plasmas, the dimensionless numbers selected for study were the effective collisionality ( $\nu_{eff}$ ) and the relative gyroradius ( $\rho^*$ ) due to their significance in Eq. 2.1.

The relative gyroradius relates the ion Larmor radius to the minor radius of the plasma and decreases when either the plasma minor radius or the magnetic field strength increases. When a charged particle is placed in a magnetic field, it moves in a circular pattern. The radius of the circle that the charged particle makes in this field is called its Larmor radius. The relative gyroradius is also linked to the  $k_{\perp}$  term in Eq. 2.1. Notably, the relative gyroradius is also the only dimensionless number linked to the electrostatic drift wave equation that depends on ion mass. In order to facilitate dimensionless relative gyroradius matches between the hydrogen and helium plasmas, the plasmas created at LAPD for this project were confined at a magnetic field of 1 kG or 2 kG. It then became possible to find effective collisionality matches and to draw conclusions about the electrostatic drift wave equation.

The formula for the relative gyroradius used in this project was derived by Kadomtsev and can be written as follows [8]:

$$\rho^* = \frac{cm_i^{1/2}T_e^{1/2}}{eaB}, \quad (2.2)$$

where  $c$  is the speed of light,  $m_i$  is the ion mass,  $T_e$  is the electron temperature,  $e$  is the electron charge,  $a$  is the plasma minor radius, and  $B$  is the magnetic field. Collisionality describes the rate of collisions, specifically electron-ion collisions, in a plasma. Increased collisionality has been linked to higher levels of turbulence [3]. Electron-ion collisions in particular play a role in Eq. 2.1. However, the dimensionless equation derived by Kadomtsev to describe collisionality in plasmas relied on bounce frequency, which is when a particle trapped between two magnetic mirrors bounces back and forth between them periodically with a specific “bounce frequency.” Because the plasmas at LAPD would not have a bounce frequency unless there was a wave in the parallel direction, this was not a useful parameter to create a dimensionless collisionality with. As a result of this, a formula for effective collisionality used in tokamaks was used instead, and can be written as follows [10]:

$$\nu_{eff} \sim \frac{.01RZ_{eff}n_e}{18T_e^2}, \quad (2.3)$$

where  $R$  is the plasma major radius,  $Z_{eff}$  is the effective ionization (assumed to be 1 for both hydrogen and helium ions in this project), and  $n_e$  is the electron density of the plasma. While both the formulas for relative gyroradius and collisionality were derived for tokamaks, LAPD can be approximated as a small part of the circumference of a large torus, so the difference in geometry does not render the equations irrelevant. In order to account for this difference in geometry, the major axis  $R$  was replaced with the minor axis  $a$  as the default “size” of the plasma.

In this paper, we aim to compare the turbulence of hydrogen and helium plasmas at LAPD by doubling the magnetic field for the helium plasmas, which lowers their

relative gyroradius values into a range where they can be matched with hydrogen relative gyroradius values. Once a relative gyroradius match is established, a collisionality match can be found, which can then be used to indicate similar levels of turbulence in each species of plasma.

# Chapter 3

## Dimensionlessly Matching Plasmas at LAPD

This chapter will explain how dimensionlessly matched plasmas at LAPD were created and analyzed. It will begin by explaining the experimental setup at LAPD. Then, it will explain the Langmuir probes used to collect data and how these measurements were used to obtain the electron temperature and density values for each plasma.

### 3.1 Experimental Setup

We obtained the data used in this project at the Large Plasma Device (LAPD) at UCLA. LAPD is a cylindrical device with a plasma column that has a maximum length of 18 meters and a maximum diameter of 75 cm. It has a barium-oxide coated cathode at one end that is used to create the plasma [11]. The plasma is confined using cylindrical magnets, which creates an axial magnetic field as shown in Fig. 3.1.

In this experiment, the Large Plasma Device began each plasma with the chamber in a near-vacuum state. Then, in a method of creating a plasma referred to as a gas puff, the cathode fired electrons into the chamber while a gas was simultaneously puffed into the chamber near the cathode. This method of creating plasmas was beneficial to this experiment because hydrogen plasmas that are created by allowing

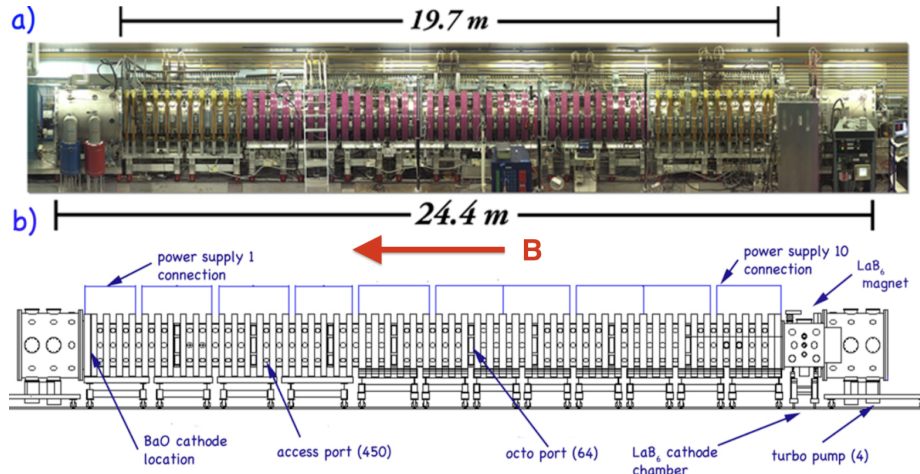


Figure 3.1: The upper image, marked as a), shows a composite photo of LAPD. The lower image, marked as b), is a labeled diagram of LAPD indicating the location of the cathode and ports. The ports run axially along the device and are located in between cylindrical magnets, which are painted yellow and purple in the photo above [11]. In this orientation, the gas would enter near the cathode and travel to the right through the chamber, while the magnetic field would point axially to the left. The high-speed camera is located at the far right end of the machine.

the chamber to fill with a uniform density of gas before the cathode activates (known as a prefill) are more challenging to create. As the purpose of this experiment is to establish and compare the end points of fully hydrogen and fully helium plasmas, the gases in this experiment consisted either entirely of helium atoms or molecular hydrogen.

As shown in Fig. 3.2, gas stopped being pumped into the chamber 30 ms into each run because it was noticed experimentally that this improved the electron temperature confinement. This slight variation in confinement was desirable since it offered more possibilities for obtaining a dimensionless match without having to spend the limited runtime allotted to this experiment on LAPD on creating a very similar plasma.

Probe measurements were taken at 1 cm intervals along the diameter of the chamber from 0 to 67 cm, as illustrated in Fig. 3.3. For each radial position, plasmas are recreated using identical operating conditions 8 times to account for random errors.

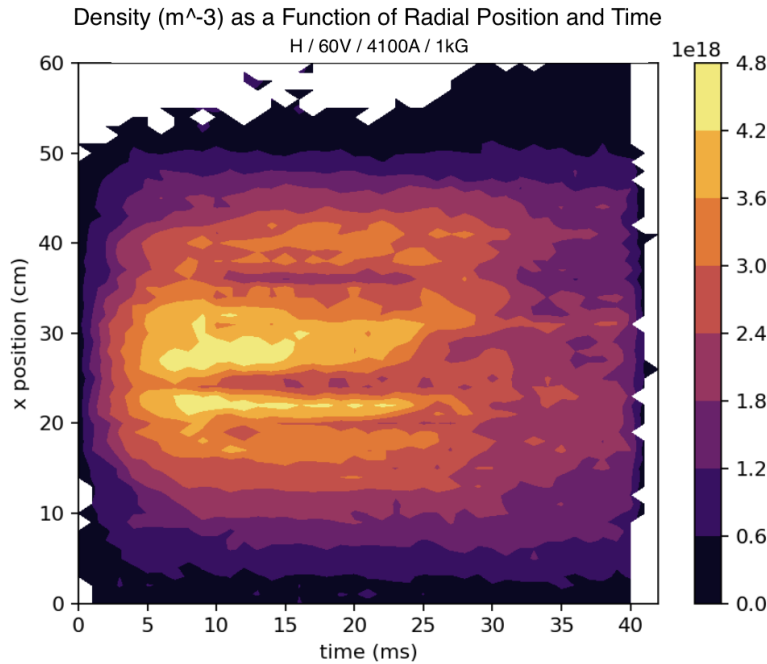


Figure 3.2: This graph shows a contour plot of the density measured in LAPD as a function of both radial position and time. Note the decrease in density after the cutoff time at 30 ms.

The Langmuir probes recorded measurements at time intervals of 1 ms at each position throughout the duration of the plasma. Each of the plasmas used for dimensionless comparisons in this project lasted for 40 ms. While previous experiments collected data for around 20 ms for each plasma, extending the lifespan made it possible to get useful information out of turning off the gas. It also helped account for experimental variation by allowing the plasma to remain in steady state for longer.

Though LAPD offers the ability to create nonuniform magnetic fields along the length of the chamber, this experiment chose to have a uniform magnetic field in the center of the chamber to better reproduce the ideal conditions for drift wave turbulence. Due to the calculations for the relative gyroradius, the hydrogen and helium plasmas were dimensionlessly matched by creating hydrogen plasmas confined by a magnetic field of 1 kG and the helium plasmas confined by a B field of 2 kG.

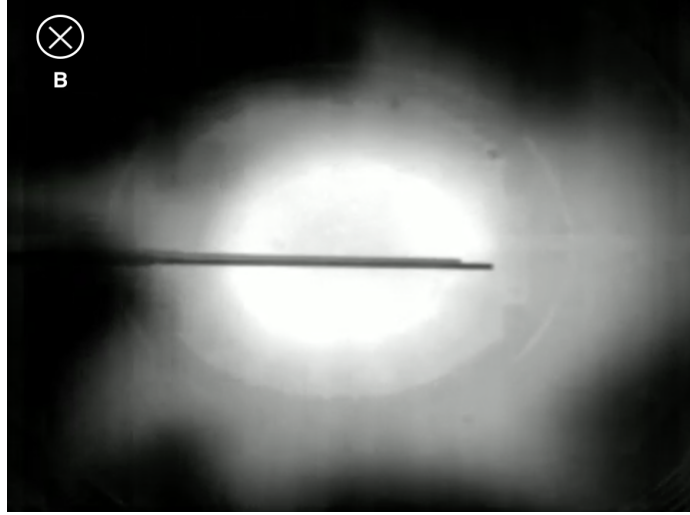


Figure 3.3: An image taken by the high-speed camera during a plasma shot. The high-speed camera is oriented so that it faces the cathode. Note the silhouettes of the probes as they protrude radially into the chamber.

Additional 1 kG helium and 2 kG hydrogen plasmas were taken for comparison.

## 3.2 Langmuir Probes

The raw data used in this project was collected using two Langmuir probes. Langmuir probes can be used to measure plasma quantities like the electron temperature and density for plasmas with short timescales and hotter temperatures than a regular thermometer would be able to measure. They operate based on the principle that plasmas consist of relatively massive, positively charged ions and much smaller negatively charged electrons. As a result, the number of electrons and ions that hit the probe can be detected as current.

Langmuir probes measure current, voltage, and time as they sweep from a strong negative voltage (around -40 V) to a strong positive voltage (around 20 V). At a strong negative voltage, the electrons are repelled from the probe and the probe measures a fairly stable positive current known as the ion saturation current, where



the maximum possible number of ions are hitting the probe. As the probe voltage increases, the electrons go from being repelled by the probe to attracted to it until an electron saturation current is reached and the current plateaus once more. This means that the plot of measured current vs. voltage is best described by an S-curve, as shown in Fig. 3.4. Since the temperature is an average of the kinetic motion of the particles in the plasma, electrons at higher temperatures will require a greater voltage to change their trajectory and start hitting the probe. This means that the gradient of the slope of the S-curve is a reflection of the electron temperature of the plasma.

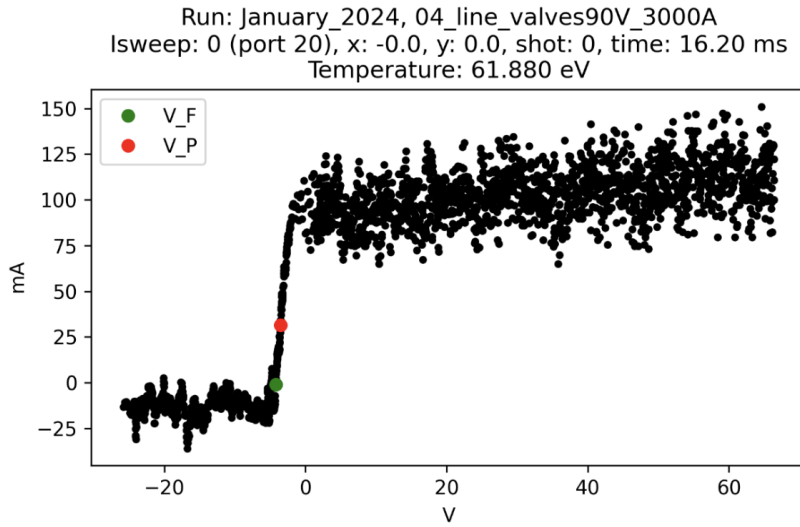


Figure 3.4: An IV sweep showing the measured current as the probe swept from a low voltage to a high voltage.  $V_f$  and  $V_p$  are the floating potential and the plasma potential respectively, and are essential to finding the electron temperature and density.

IV sweep measurements (also sometimes referred to as “ramps”) were taken at millisecond intervals throughout the duration of the plasma as seen in Fig. 3.5. This provided the time resolution for the electron temperature and density data in this project. Langmuir probe measurements were taken in two locations along the length

of the device, with the “upstream” location being at the axial port 20 and the “downstream” location at axial port 29.

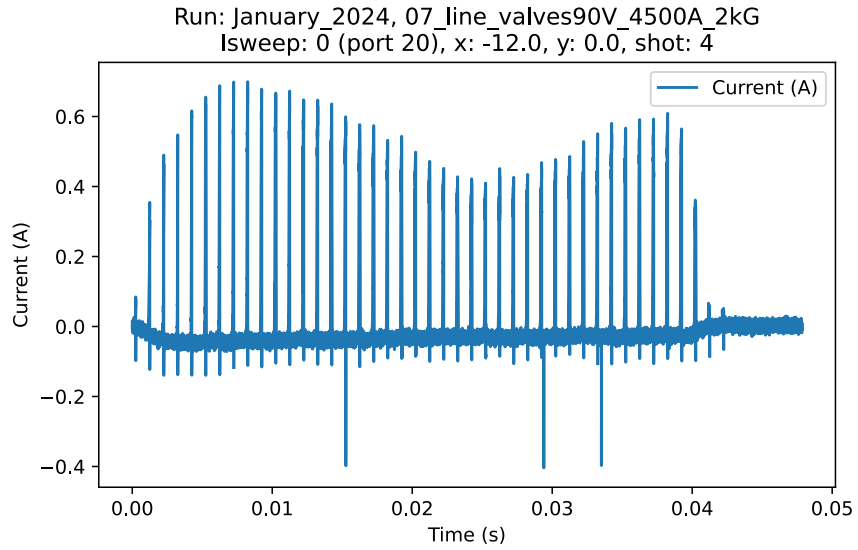


Figure 3.5: This graph shows a plot of the current measured by a Langmuir probe over time for a single plasma shot. Each current spike corresponds to an IV sweep. This means that the frequency of these current spikes indicate the time resolution of the density and temperature data in this experiment (1 ms).

### 3.3 Obtaining Electron Temperature and Density from Langmuir Probes

The first step taken to analyze the data from this experiment was to extract the bias, current, and time information. The data then had units attached to it and also accounted for any consistent DC offset the probe might have. Then each individual IV sweep was isolated from the data surrounding it for further analysis.

The most important parts of an IV sweep for electron temperature and density analysis are the floating potential, the plasma potential, and the electron and ion saturation currents. The floating potential is the point at which the current crosses 0. It is used as a cutoff point for the analysis used to find the plasma potential and the electron temperature. The plasma potential is the point of steepest slope on the IV sweep. It contains important information about temperature. The electron saturation current is the part of the IV sweep that plateaus at its highest possible current. The ion saturation current is below 0 on an IV sweep and is the plateau at the bottom of the S curve.

The electron temperature can roughly be calculated from the following equation:

$$\ln|I_{\text{probe}} - I_{\text{sat}}| = \frac{e}{k_B T_e} (V_{\text{bias}} - V_f) + \text{const.} \quad (3.1)$$

Where  $I_{\text{probe}}$  is the raw current recorded by the probe,  $I_{\text{sat}}$  is the saturation current,  $e$  is the charge of an electron,  $k_B$  is the Boltzmann constant,  $T_e$  is the electron temperature,  $V_{\text{bias}}$  is the plasma potential, and  $V_f$  is the floating potential. Once the electron temperature is found, it can be used to calculate the electron density as follows:

$$n_e = \frac{4I_{\text{sat}}}{A_p e v_{th}} \quad (3.2)$$

where  $A_p$  is the probe area and  $v_{th} = \sqrt{\frac{8T_e}{\pi m_e}}$ . This method of calculating electron density relies on the electron saturation current  $I_{sat}$ , which can be written as follows:

$$I_{sat} = \frac{1}{4} e n_e A_p \sqrt{\frac{8T_e}{\pi m_e}} \quad (3.3)$$

where  $n_e$  is the electron density and  $m_e$  is the electron mass.

These two formulas were implemented by PlasmaPy in order to extract electron temperature and density. However, as shown in Fig. 3.4, the raw current data collected by the Langmuir probe can have a great deal of noise. This noise becomes more prevalent at the edges of the plasma and at the beginning and end of the plasma shot. Due to the fact that the plasma potential and the floating potential depend on finding the point of steepest slope on the S-curve and where the S-curve crosses 0 current respectively, having noise with steep slopes that could prematurely cross the 0-current threshold is problematic for analysis.

There were several possible ways to mitigate this issue. Curve-fitting, splining, and smoothing the noise using a moving average were all tried to reduce the impact of noise on the analysis, as shown in Fig. 3.6. While the moving average was the best option of these three due to the fact that it could account for the occasionally Bimaxwellian nature of the S-curve, it did not perform particularly well on curves with a very steep slope since the moving average would smooth it out to a significant degree.

However, in the end the most effective method was a histogram bin method that involved sorting the current into histogram bins and finding the point of steepest slope by finding which bin had the smallest value, since fewer data points would be in the range of currents that changes the fastest. This improved the noise tolerance of the code since it depended on the distribution of current values rather than the slope

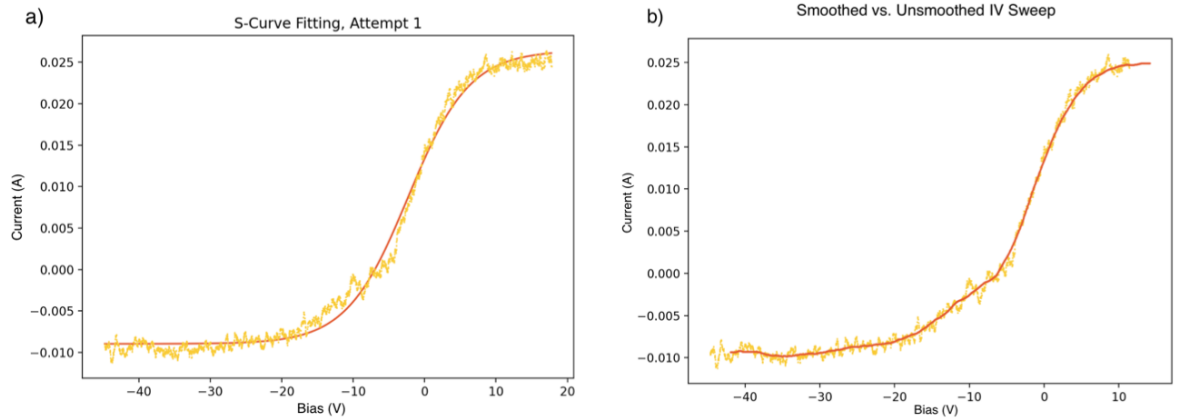


Figure 3.6: This figure shows comparisons between raw current data from an IV sweep and a) an attempt at fitting that IV sweep with an S-curve, which fails due to the Bimaxwellian knee of the plasma and b) the same IV sweep but with a smoothing margin.

between two points or taking broad averages. While this method is still imperfect since it assumes that the bias is equally spaced, it enabled the usage of many IV sweeps with strong S-curves but large amounts of noise such as those in Fig. 3.4. The  $V_f$  and  $V_p$  markers indicate where the code pulled out the floating potential and the plasma potential.

Once  $V_f$ ,  $V_p$ ,  $I_{sat}$ , and  $I_{probe}$  were extracted from the IV sweeps, they were plugged into Eqs. 3.1 and 3.2 to get the electron temperature and density. The electron temperatures and densities were then averaged over each of the 8 discharges and plugged into Eqs. 2.2 and 2.3. These relative gyroradius and collisionality values were then organized into radial profiles taken at specific times during the lifespan of the plasma. The radial profiles were then compared to find the closest dimensionless match.

Plasmas at LAPD were created 8 times under identical operating conditions for each spatial and temporal data point in order to create profiles for each plasma. The

data from each of these discharges was collected using a Langmuir probe, which is able to extract information about the electron temperature and density of the plasma from the current it measures as it sweeps from a low voltage to a high voltage. Once the data was processed to reduce the impact of noise on the analysis, electron temperature and density values were obtained.

# Chapter 4

## Comparing Hydrogen and Helium Plasmas

This chapter will discuss the two relative gyroradius and collisionality matches found at LAPD. It will also discuss the relationship between the dimensionless numbers and the temperature and density profiles for the matched plasmas. It will then discuss two plasmas where only one dimensionless parameter was matched. Then, it will compare the hydrogen to helium ratios of temperature, density, relative gyroradius, effective collisionality, and turbulence growth rate values for all four matches. Afterwards, it will show the way that the collisionalities of hydrogen plasmas decreased while the collisionalities of helium plasmas increased when exposed to an increased magnetic field. It will then describe the normalized density gradients calculated at the edge of the plasmas.

### 4.1 Dimensionless Matches

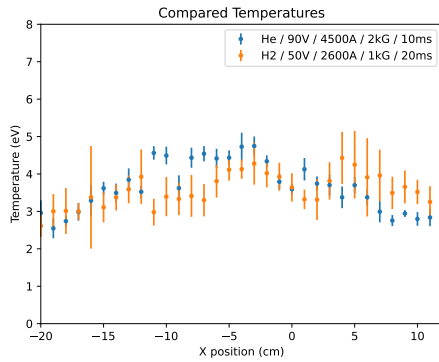
Temperature and density profiles were created for each plasma using the data collected from the Langmuir probes. These profiles consisted of the average of the temperature and density over the 8 discharges of the plasma at specific locations and times, as shown in Fig. 4.1. The profiles used in this project are radial profiles, meaning they

illustrate the temperature and density across the diameter of the cylindrical cross-section of LAPD. Each profile also corresponds to a specific time in milliseconds during the lifespan of the plasma. As can be seen in Fig. 4.1, the hydrogen densities were consistently lower than the helium densities in all the plasmas studied in this project.

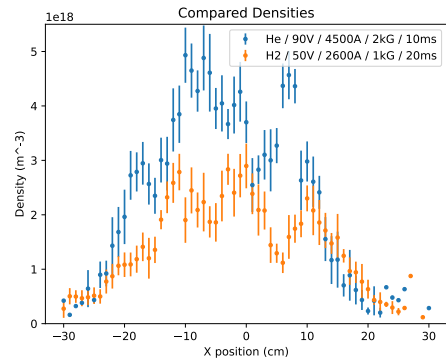
As evidenced by the error bars in Fig. 4.2, the temperature data was variable to the point of unreliability beyond the core of the plasma (-20 cm to 12 cm). As such, the graphs of the temperature profiles were limited to looking at the core of the plasma in order to better visually characterize the physically significant aspects of the data. All calculations based on temperature were also limited to this range. However, the density data was reliable at the edges of the plasma, which is why the x-axes of the density graphs display the entire diameter of LAPD's central chamber.

Two dimensionless matches were found between hydrogen and helium plasmas, as shown in Fig. 4.3. These matches were found by plugging temperature and density values in to Eq. 2.2 and Eq. 2.3 to create profiles for the relative gyroradii and collisionalities for the hydrogen and helium plasmas, which were used to identify dimensionless matches at specific times during the lifespan of the plasma. As can be seen comparing Fig. 4.1 with Fig. 4.3, the relationship between the hydrogen and helium electron temperatures and the relationship between their relative gyroradii are proportionate to one another. This is reasonable because the plasma's electron temperature is the only non-constant and unmatched value in Eq. 2.2. However, the collisionality depends on both temperature and density, meaning that the collisionality does not directly reflect either one of them individually. Because the collisionalities depend on both temperature and densities, error propagation caused the error bars in the collisionalities to be substantially larger than the error bars in any of the other profiles. However, the fluctuations of the collisionalities are substantially smaller than

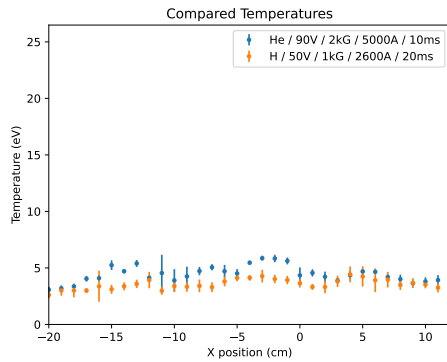




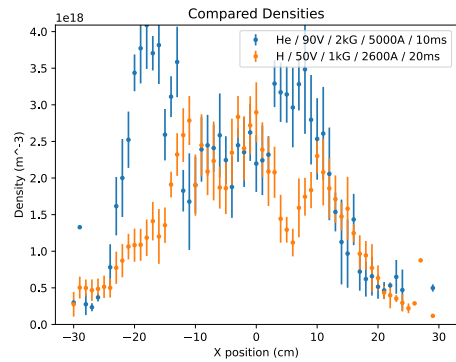
(a) This graph shows the temperature profiles of the first dimensionless match found at LAPD.



(b) This graph shows the density profiles of the first dimensionless match found at LAPD.



(c) This graph shows the temperature profiles of the second dimensionless match found at LAPD.



(d) This graph shows the density profiles of the second dimensionless match found at LAPD.

Figure 4.1: Temperature and density profiles of the relative gyroradius and collisionality dimensionless matches

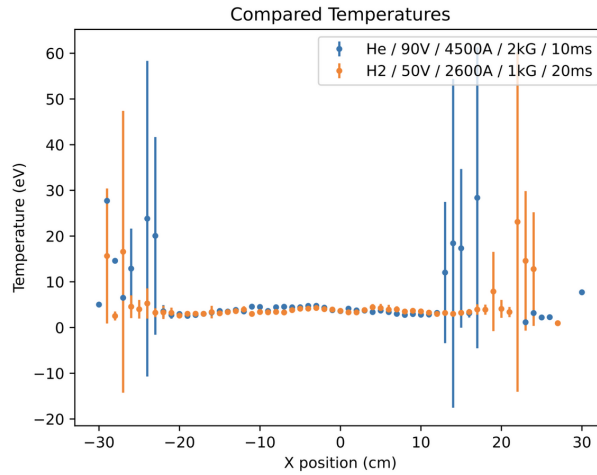
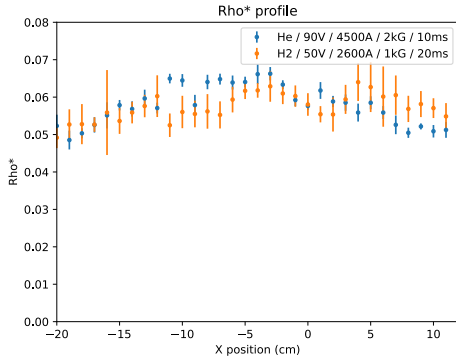


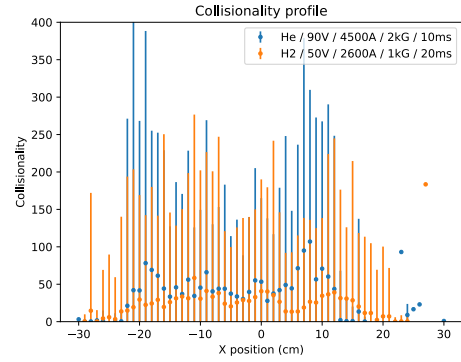
Figure 4.2: This graph illustrates the unreliability of the temperature data outside the core of the plasma due to variations in the temperature data for each discharge.

the size of the error bars, indicating that the error bars overestimate the unreliability of the calculated collisionality values.

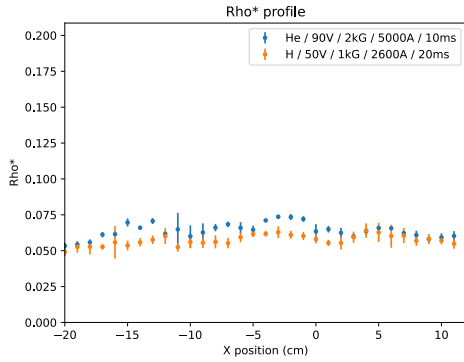
As expected, the only joint relative gyroradius and collisionality matches were found when the helium plasmas were confined with a magnetic field of 2 kG and the hydrogen plasmas were confined with a magnetic field of 1 kG. Within each relative gyroradius match, there were ranges of collisionalities, some of which were closer to a match than others. The closest match found so far is shown with Dimensionless Match 2 as can be seen in 4.3. This can also be seen in Table 4.1, where the hydrogen/helium collisionality ratio in Dimensionless Match 1 is shown to be approximately .55. This is likely due to collisionality spikes near the edge gradient regions of the helium plasma, which can be seen in Fig. 4.3b.



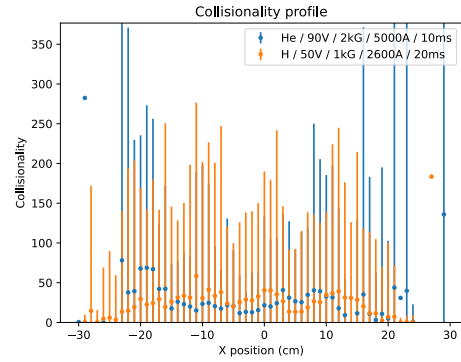
(a) This graph shows a relative gyroradius match between the first pair of dimensionlessly matched plasmas.



(b) This graph shows a collisionality match between the first pair of dimensionlessly matched plasmas.



(c) This graph shows a relative gyroradius match between the second pair of dimensionlessly matched plasmas.



(d) This graph shows a collisionality match between the second pair of dimensionlessly matched plasmas.

Figure 4.3: Radial profiles of the relative gyroradius and collisionality dimensionless matches

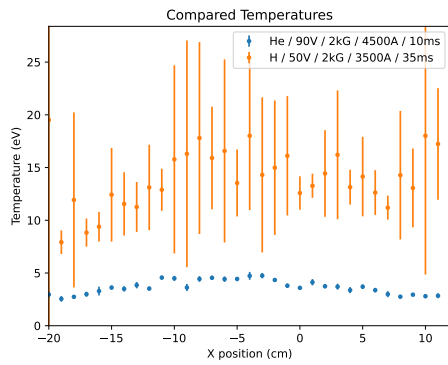
## 4.2 Partial Dimensionless Matches

In order to isolate the effects of each dimensionless parameter on the system, radial profiles with a poor relative gyroradius match and a good collisionality match were examined. Radial profiles with a good relative gyroradius match and a poor collisionality match were also studied. Unexpectedly, these partial dimensionless matches occurred when the hydrogen and helium plasmas were subjected to the same strength of magnetic field.

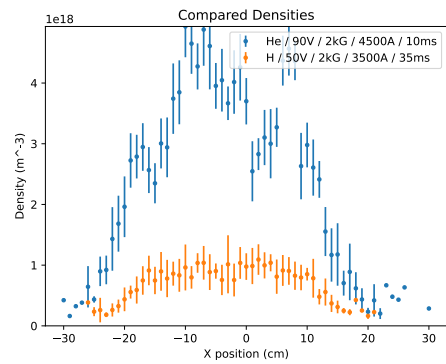
Looking at the temperatures in Fig. 4.4, the relative gyroradius-only match was due to the hydrogen plasma being approximately 3.8 times the temperature of the helium plasma. However, the temperatures for the collisionality match are approximately the same. This explains part of why the relative gyroradius values were different for the collisionality-only match in Fig. 4.5, since the factor of 2 introduced by the different ion mass was not mitigated by either the magnetic field or an increase in electron temperature. It is also notable that the hydrogen density appears to decrease while the helium density appears to increase in the relative gyroradius-only match, when both plasmas are at 2 kG.

## 4.3 Calculating the Turbulence Growth Rate

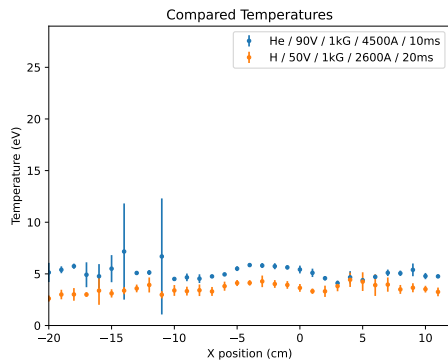
Once the dimensionless matches were found, the average  $\rho^*$ , effective collisionality, density, and temperature were evaluated over the core region of the plasma (-20cm to 12cm) to quantitatively compare the plasmas to one another. For each of these values in every dimensionless match, a ratio was taken between the hydrogen and helium plasmas in order to gauge the effectiveness of the match. In order to determine the extent to which the turbulences of each plasma matched, the effective collisionality, relative gyroradius, and temperature were multiplied together proportionately to how



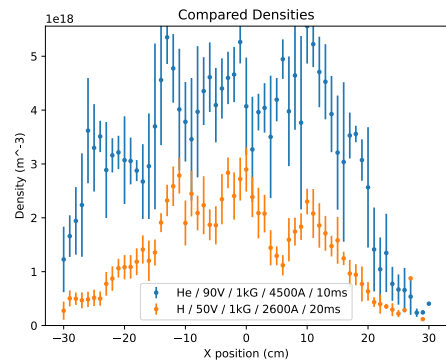
(a) This graph shows the temperature profiles for the relative gyroradius-only match.



(b) This graph shows the density profiles for the relative gyroradius-only match.

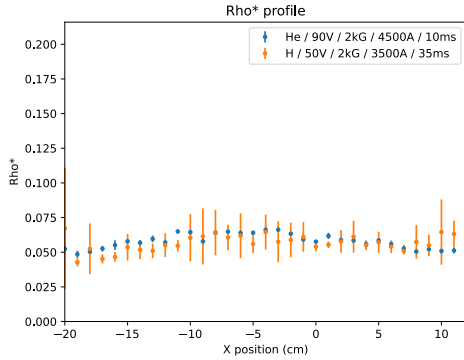


(c) This graph shows the temperature profiles for the collisionality-only match.

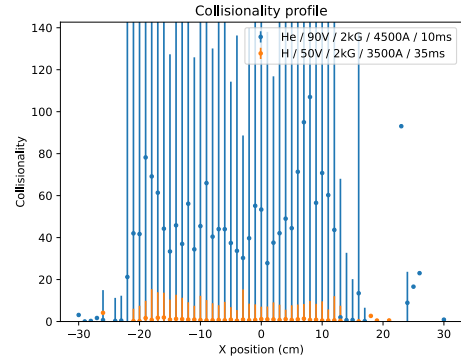


(d) This graph shows the density profiles for the collisionality-only match.

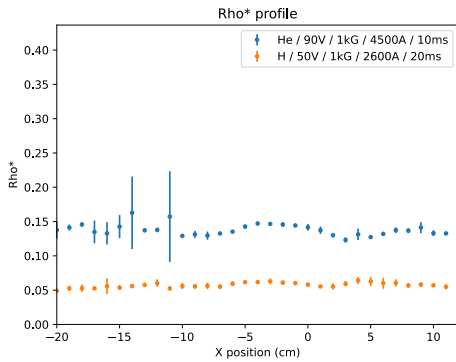
Figure 4.4: Temperature and density profiles for the relative gyroradius-only and collisionality-only matches



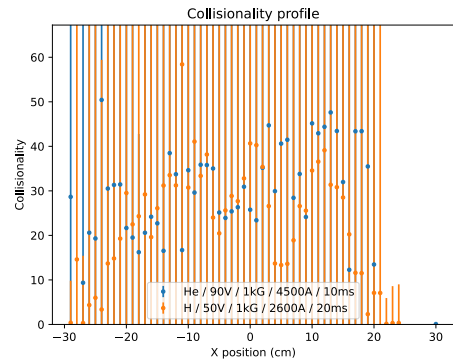
(a) This graph shows the relative gyroradius match for the hydrogen and helium plasmas that were chosen to only have a strong relative gyroradius match.



(b) This graph shows the collisionality match for the hydrogen and helium plasmas that were chosen to only have a strong relative gyroradius match.



(c) This graph shows the relative gyroradius match for the hydrogen and helium plasmas that were chosen to only have a strong collisionality match.



(d) This graph shows the collisionality match for the hydrogen and helium plasmas that were chosen to only have a strong collisionality match.

Figure 4.5:  $\rho^*$  and collisionality profiles for the relative gyroradius-only and collisionality-only matches

they appear in Eq. 2.1. The electron temperature was included in this calculation because  $v_{th} = \sqrt{\frac{8T_e}{\pi m_e}}$ , which means that  $v_{th}$  cannot be taken as a constant between the two plasmas. For simplicity, all values assumed to be constant between the hydrogen and helium plasmas were neglected from the comparison. The ratios of hydrogen and helium temperature, density,  $\rho^*$ ,  $\nu_{eff}$ , and turbulence growth rate values can be seen in Table 4.1.

	Temperature (eV)	Density ( $\text{m}^{-3}$ )	$\rho^*$	$\nu_{eff}$	Turbulence growth rate
Dimensionless match 1	.97	.57	.98	.55	.31
Dimensionless match 2	.82	.71	.89	1	.97
$\rho^*$ only match	3.8	.25	.98	.017	7.8e-05
Collisionality only match	.69	.49	.41	1	.24

Table 4.1: This table shows the H/He ratio of the average temperature, density,  $\rho^*$ ,  $\nu_{eff}$ , and turbulence growth rate values evaluated over the core of the plasma (-20 cm to 12 cm).

As evidenced by Table 4.1, Dimensionless Match 2 was the best dimensionless match overall with a H/He turbulence growth rate ratio of .97. Dimensionless Match 1 had the second closest turbulence growth factor match, but with a substantially worse value of .31. The collisionality-only match was only slightly worse off with a value of .24, while the relative gyroradius-only match was by far the worst growth factor match at 7.8e-05. This indicates that collisionality matches have a greater impact on the quality of the turbulence growth rate match, likely due to the fact that collisionality values ranged from 19-900 times larger than their corresponding relative gyroradius values. Considering the fact that the squares of both the relative gyroradius and collisionality are in the numerator in Eq. 2.1, it is reasonable that the term with the greater magnitude would dominate.

## 4.4 Impact of the Magnetic Field on Collisionality

Comparing the collisionalities in the relative gyroradius-only match with the collisionality-only match gave rise to an unexpected result: when exposed to a heightened magnetic field, the collisionality of the hydrogen and helium plasmas behaved in opposite ways. In order to verify this finding, we studied the collisionalities of hydrogen and helium plasmas that were created with nearly identical operating parameters at 1 kG and 2 kG, as can be seen in Figs. 4.6 and 4.7. These findings matched up with what was previously observed in the collisionality-only and relative gyroradius-only matches—hydrogen collisionalities decreased in the presence of an increased magnetic field, while helium collisionalities increased.

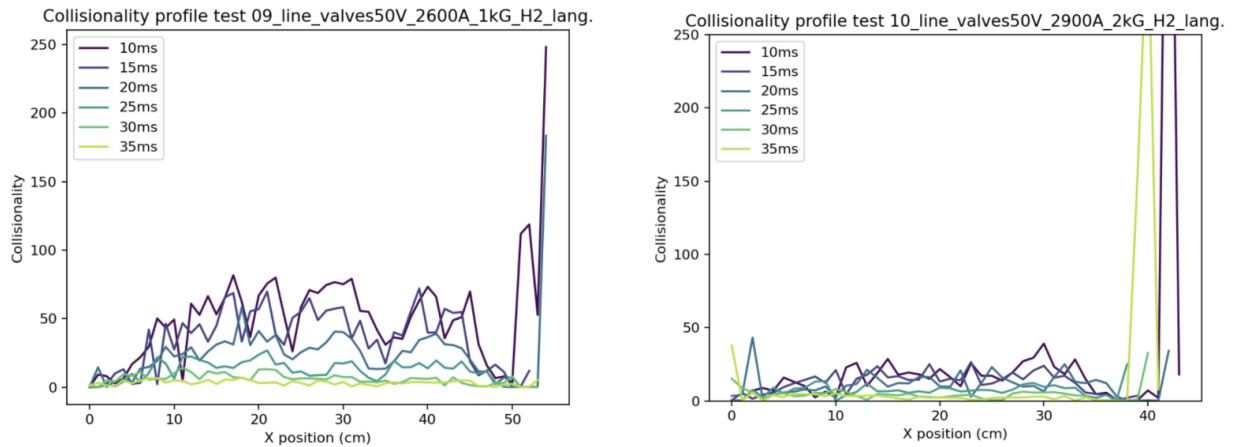


Figure 4.6: This graph shows how the average collisionality decreases in otherwise similar hydrogen plasmas when the magnetic field is raised from 1 kG to 2 kG.

As shown in Eq. 2.3, the effective collisionality of the plasma depends on both the electron density and the electron temperature. However,  $T_e$  has a greater impact on the effective collisionality due to the fact that it's raised to a higher power. This means that while the collisionality is sensitive to changes in density, changes in temperature will have a larger effect on the collisionality of the system. Higher elec-



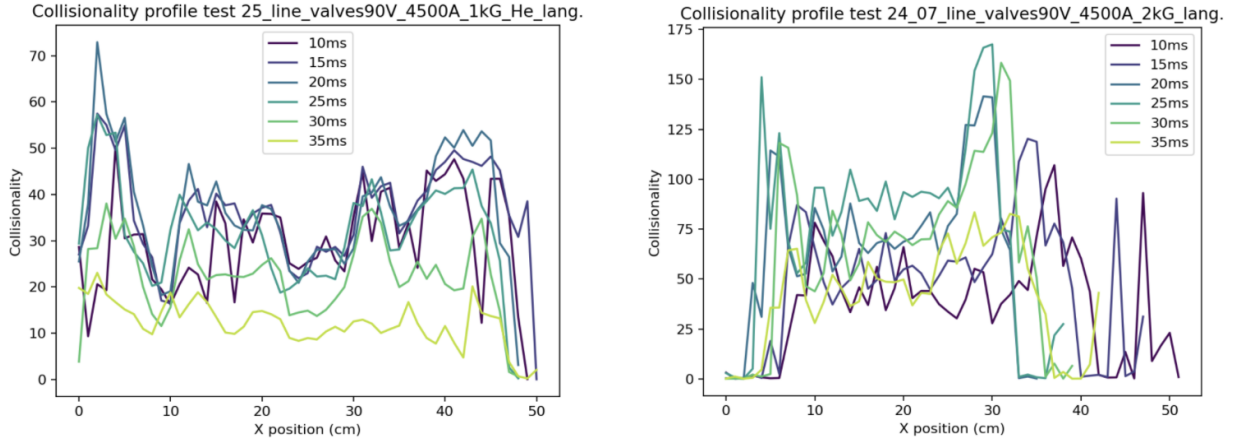


Figure 4.7: This graph shows how the average collisionality rises in otherwise identical helium plasmas when the magnetic field is raised from 1 kG to 2 kG.

tron temperatures will lead to lower collisionalities, while higher densities will lead to higher collisionalities.

It is also important to avoid neglecting changes in density due to the increased magnetic field. As is evident in the density profiles of all four dimensionless matches, the helium densities were consistently higher than their hydrogen counterparts, though as evidenced in Table 4.1 they were closest in Dimensionless Match 1 and Dimensionless Match 2. It was also observed in the relative gyroradius match that when the magnetic field of the hydrogen increased from 1 kG to 2 kG, the density in the core of the plasma was less than the 1 kG hydrogen plasma densities in the other matches. While this was also observed with helium when comparing the 1 kG helium plasma in the collisionality match with the other 2 kG helium plasmas, the 2 kG helium plasmas were approximately  $\frac{3}{4}$  that of the 1 kG helium plasma while the 2 kG hydrogen plasma was roughly  $\frac{1}{2}$  of their 1 kG counterparts. This could be responsible for some of the discrepancy in the behavior of the collisionalities.

## 4.5 Comparing the Density Gradients of Dimensionlessly Matched Plasmas

Since an increase in turbulence causes a decrease in the effectiveness of magnetic confinement, information about the turbulence in a plasma can be gained by observing the density gradients at the edges of the plasma. Gradual normalized gradients are indicative of more turbulent plasmas, while the inverse indicates lessened turbulence. Once a dimensionless match was found, the bounds of the edge gradient were identified and a linear fit was applied to it, as shown in Fig. 4.8. The slope was then normalized by the average value of the gradient in that range.

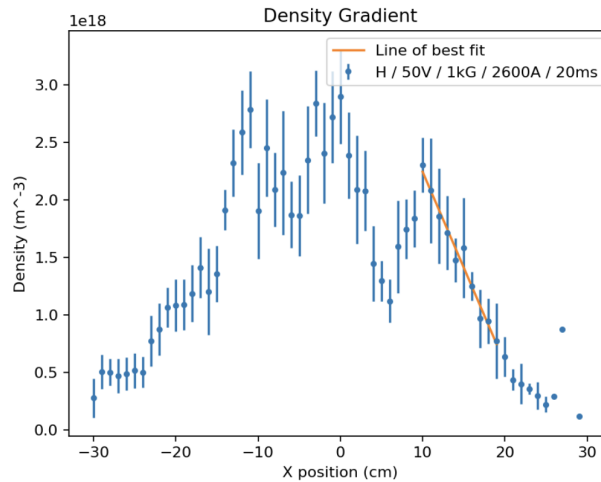


Figure 4.8: This graph illustrates the linear fit of the density gradient. The slope of and average density of this gradient was then used to find the normalized density gradient.

It has been observed before in previous experiments at LAPD that the radial density profiles are not symmetric, with the right-hand side of the radial profile being deemed more reliable [12]. This can also be observed in Fig. 4.8. This project also limited its study to the right side of the radial profile of the device. The normalized density gradients for the right hand side of the radial profiles can be seen in Table 4.2.

	Hydrogen Normalized Density Gradient	Helium Normalized Density Gradient	H/He Ratio
Dimensionless match 1	-0.12	-0.22	.55
Dimensionless match 2	-0.12	-0.18	.67
$\rho^*$ only match	-0.15	-0.22	.68
Collisionality only match	-0.12	-0.085	1.4

Table 4.2: This table shows the normalized density gradients for the totally and partially dimensionlessly matched plasmas.

It is interesting to note that both dimensionless matches and the  $\rho^*$  match have hydrogen normalized density gradients that are between .5-.7 times that of the helium normalized density gradients. However, there is a notable exception for the collisionality-only match, where the helium normalized density gradient is less than half of all the other helium normalized density gradients, resulting in a H/He ratio of 1.4. While it would take more experimental evidence to determine whether this is a consistent pattern or a singular occurrence, it could indicate that helium plasmas confined at 1kG are even less confined than hydrogen plasmas at 1kG. As expected, the hydrogen normalized density gradient was steeper when it was confined by a magnetic field of 2kG in the  $\rho^*$ -only match. As expected, Dimensionless Match 2 had the closest H/He normalized density gradient ratio. However, the normalized density gradient ratios of the other dimensionless matches did not follow the same trend displayed in Table 4.1. This could indicate that either the normalized density gradients do not fully describe the turbulence in the plasma or that there are additional factors affecting the turbulence in the plasma that are not yet accounted for.

In order to establish a baseline for analyzing mixed hydrogen and helium plasmas, this project set out to compare the turbulence in hydrogen and helium plasmas at LAPD using dimensionless numbers. The relative gyroradius dimensionless parameter

values were matched experimentally by raising the magnetic field confining the helium from 1 kG to 2 kG. After completing analysis of the Langmuir probe data, relative gyroradius, and collisionality values for the different plasma runs were calculated and compared against one another. For the closest match, the electron temperature largely reflected the relative gyroradius values. The slope of the hydrogen density at the edges of the plasma was more gradual than the density slope of the helium plasma. It was also discovered that the collisionalities of hydrogen and helium plasmas did not respond in the same way to increased magnetic confinement—the collisionalities of otherwise similar hydrogen plasmas dropped under the increased magnetic field, whereas the helium collisionalities rose. It was observed that while the turbulence growth rates behaved as expected, the normalized density gradients did not reflect the same patterns displayed by the turbulence growth rates, which indicates that some physical insight into the turbulence or the normalized density gradients is missing.

# Chapter 5

## Discussion

This chapter will summarize the results of the experiment and will discuss open questions that remain after the analysis, as well as suggesting ways that those open questions could potentially be answered. It will also discuss experimental errors that could be mitigated by repeated experimentation. Finally, it will describe how this experiment could be built off of in order to fulfill its goal of understanding the extent to which mixing hydrogen and helium plasmas affect turbulence.

The overall goal of this project was to find a dimensionless match between a hydrogen and helium plasma created at LAPD. This goal was successfully accomplished—two dimensionless matches were found in plasmas that had similar operating parameters. The hydrogen run in both matches was the same, while the only difference in the helium runs was a 500 A difference in the amount of current running to the cathode. Dimensionless Match 2 was a better match than Dimensionless Match 1 since Dimensionless Match 1 had non-outlier collisionality fluctuations in the core of the plasma, which caused the average collisionalities to differ by a factor of approximately 1.8. The reliability of Dimensionless Match 1 could be verified through further experimentation to determine if the collisionality issues persisted or were a singular phenomenon. As expected, both of these matches occurred when the helium plasmas were confined by a magnetic field of 2 kG and the hydrogen plasmas were

confined by a magnetic field of 1 kG.

However, partial dimensionless matches were observed where only one of the two dimensionless parameters aligned when both plasmas were confined by the same strength of magnetic field. The relative gyroradius-only match occurred when both plasmas were confined by a magnetic field of 2 kG, while the collisionality-only match occurred when both plasmas were confined by a magnetic field of 1 kG.

Observing how the collisionalities changed between the relative gyroradius-only match and the collisionality-only match gave rise to an unexpected result: hydrogen collisionalities decreased in the presence of an increased magnetic field, while helium collisionalities increased in an increased magnetic field. It is important to note that the helium densities appear to increase in the heightened magnetic field while the hydrogen densities decrease, and the helium temperatures appear to slightly decrease while the hydrogen temperatures increase. While the mechanism responsible for this divergence in the behavior of the two species of plasma remains unknown, this behavior suggests that increasing the magnetic field increases particle confinement in helium plasmas and energy confinement in hydrogen plasmas, which would explain the difference in their collisionalities. One way to test our understanding of this behavior would be attempting to recreate this behavior using simulations. The simulations could then be verified by further experiments.

The drift wave turbulence growth rates calculated using the average values taken over the core of the plasma behaved as expected—the closer the dimensionless match was, the closer the turbulence growth rate match became. However, these results did not match with the normalized density gradients, which serve as an alternative way to observe the extent to which turbulence is affecting the plasma. While Dimensionless Match 2 was the closest match in both instances, the closeness of the other matches varied significantly. This indicates that some physical insight into either the

turbulence or the density gradients is missing. One way to fill in this gap in our understanding would be to analyze data collected from 4-tipped Langmuir probes, which are capable of studying turbulence more directly.

There were also several experimental factors that increased the errors and irregularities of this experiment. There were more variations in the plasma density than originally expected, which leads to a degree of uncertainty in the validity of the collisionality matches. It is possible that the error bars could also be reduced through more sophisticated error propagation since the fluctuations in the collisionality data are substantially smaller than the data's error bars. There are some signs that the cathode was not adequately coated in barium-oxide such as the asymmetrical variations in temperature and density, which could also be responsible for irregularities in the plasma. These errors could likely be accounted for or overcome through further experimentation.

This research could be continued by investigating how the turbulence changes when the two ion species are mixed together in varying amounts. If the turbulence also changes nonlinearly like the thermal energy stored in the plasma changed in King et al.'s experiment as shown in Fig. 1.1, it could lead to meaningful improvements in existing models of astrophysical phenomenon such as the solar wind. Perhaps even more importantly than that, it could offer previously missing insight into some of the fundamental workings of plasma turbulence.

# Appendix A

## File Names and Times of Dimensionless Matches

### Dimensionless match 1:

Hydrogen: 09\_line\_valves50V\_2600A\_1 kG\_H2 at 20ms, isweep = 1

Helium: 07\_line\_valves90V\_4500A\_2 kG at 10ms, isweep = 1

### Dimensionless match 2:

Hydrogen: 09\_line\_valves50V\_2600A\_1 kG\_H2 at 20ms, isweep = 1

Helium: 06\_line\_valves90V\_5000A\_2 kG at 10ms, isweep = 1

### $\rho^*$ match:

Hydrogen: 11\_line\_valves50V\_3500A\_2 kG\_H2\_lang.nc at 35ms, isweep = 1

Helium: 07\_line\_valves90V\_4500A\_2 kG at 10ms, isweep = 1

### Collisionality match:

Hydrogen: 09\_line\_valves50V\_2600A\_1 kG\_H2 at 20 ms, isweep = 1

Helium: 25\_line\_valves90V\_4500A\_1 kG\_He at 10 ms, isweep = 1



# Bibliography

- [1] Yogesh, D Chakrabarty, and N Srivastava. “Evidence for Distinctive Changes in the Solar Wind Helium Abundance in Solar Cycle 24.” *Monthly Notices of the Royal Astronomical Society: Letters* 503, no. 1 (May 1, 2021): L17–22. <https://doi.org/10.1093/mnrasl/slab016>.
- [2] King, D. B., E. Viezzer, I. Balboa, M. Baruzzo, E. Belonohy, J. Buchanan, I. S. Carvalho, et al. “Mixed Hydrogen-Deuterium Plasmas on JET ILW.” *Nuclear Fusion* 60, no. 9 (August 2020): 096030. <https://doi.org/10.1088/1741-4326/aba452>.
- [3] Fujisawa, Akihide. “Review of Plasma Turbulence Experiments.” *Proceedings of the Japan Academy. Series B, Physical and Biological Sciences* 97, no. 3 (March 11, 2021): 103–19. <https://doi.org/10.2183/pjab.97.006>.
- [4] Chen, Francis. *Introduction to Plasma Physics and Controlled Fusion*. 3rd ed. Springer, n.d.
- [5] Ting, David. *Basics of Engineering Turbulence*. Academic Press, 2016.
- [6] Goldston, Robert, and Paul Rutherford. *Introduction to Plasma Physics*. Institute of Physics Pub., 1995.

- [7] Petty, C. C. “Sizing up Plasmas Using Dimensionless Parameters.” *Physics of Plasmas* 15, no. 8 (August 27, 2008): 080501.  
<https://doi.org/10.1063/1.2961043>.
- [8] Kadomtsev, Boris Borisovich. “Tokamak plasma : a complex physical system.” (1992).
- [9] Leishman, J. Gordon. “Dynamic Similarity,” January 1, 2023.  
<https://doi.org/10.15394/eaglepub.2022.1066.n14>.
- [10] Angioni, C, E Fable, M Greenwald, M Maslov, A G Peeters, H Takenaga, and H Weisen. “Particle Transport in Tokamak Plasmas, Theory and Experiment.” *Plasma Physics and Controlled Fusion* 51, no. 12 (December 1, 2009): 124017.  
<https://doi.org/10.1088/0741-3335/51/12/124017>.
- [11] Gekelman, W., P. Pribyl, Z. Lucky, M. Drandell, D. Leneman, J. Maggs, S. Vincena, et al. “The Upgraded Large Plasma Device, a Machine for Studying Frontier Basic Plasma Physics.” *The Review of Scientific Instruments* 87, no. 2 (February 2016): 025105. <https://doi.org/10.1063/1.4941079>.
- [12] Perks, Conor, Saskia Mordijck, Troy Carter, Bart Van Compernelle, Stephen Vincena, Giovanni Rossi, and David Schaffner. “Impact of the Electron Density and Temperature Gradient on Drift-Wave Turbulence in the Large Plasma Device.” *Journal of Plasma Physics* 88, no. 4 (August 2022): 905880405. <https://doi.org/10.1017/S0022377822000630>.